frontiers in Chemistry

ORIGINAL RESEARCH
published: 29 July 2020
doi: 10.3389/fchem.2020.00590

Flowerlike Tin Diselenide Hexagonal Nanosheets for High-Performance Lithium-Ion Batteries

Qiyao Yu[1], *Bo Wang*[2]*, *Jian Wang*[2], *Sisi Hu*[2], *Jun Hu*[1] and *Ying Li*[1]*

[1] Institute of Advanced Structure Technology, Beijing Institute of Technology, Beijing, China, [2] School of Materials Science and Engineering, Hebei University of Science and Technology, Shijiazhuang, China

$SnSe_2$ nanosheet is a common anode for lithium-ion batteries (LIBs), but its severe agglomeration hinders its practical application. Herein, a three-dimensional (3D) $SnSe_2$ nanoflower (F-$SnSe_2$) composed of non-stacking vertical upward hexagonal nanosheets was prepared through a colloidal method as an anode material for LIBs. Benefiting from the advantages of fast reaction-diffusion kinetics and buffering unavoidable volume variation during cycling, the F-$SnSe_2$ electrode displays remarkable specific capacity of 795 mAh g^{-1} after 100 cycles at 100 mA g^{-1} and superior rate performance (282 mAh g^{-1} at 2,000 mA g^{-1}). This work provides an effective way to get non-stacking nanosheets in energy storage field.

Keywords: $SnSe_2$, non-stacking, fast ion transfer, nanosheet, lithium-ion battery

OPEN ACCESS

Edited by:
Yuxin Tang,
University of Macau, China

Reviewed by:
Mingzhe Chen,
Korea University, South Korea
Xifei Li,
Xi'an University of Technology, China
Junchao Zheng,
Central South University, China

***Correspondence:**
Bo Wang
wangbo1996@gmail.com
Ying Li
bitliying@bit.edu.cn

Specialty section:
This article was submitted to Electrochemistry, a section of the journal Frontiers in Chemistry

Received: *10 April 2020*
Accepted: *08 June 2020*
Published: *29 July 2020*

Citation:
Yu Q, Wang B, Wang J, Hu S, Hu J and Li Y (2020) Flowerlike Tin Diselenide Hexagonal Nanosheets for High-Performance Lithium-Ion Batteries. Front. Chem. 8:590. doi: 10.3389/fchem.2020.00590

INTRODUCTION

In recent years, lithium-ion batteries (LIBs) have been widely employed as an energy storage system for portable electronic devices and electric or hybrid vehicles (EVs) due to their high energy density (Jiang et al., 2019; He et al., 2020). However, current LIBs are still hard to satisfy the stringent demand for security, capacity, and cost (Chu et al., 2019; Wang et al., 2019). The anode material is one of the most crucial components that can determine the battery performance directly. Recently, a variety of electrode materials, such as carbon, alloys, and transition metal chalcogenides (TMDs), have been widely investigated as anode materials for LIBs (Chen K. et al., 2018; Zhang et al., 2019; Li et al., 2020). Typically, as one of the most promising anode candidates, Sn-based materials have attracted great attention due to their high theoretical capacity and abundant resource (Lee and Park, 2017). Besides, Se-based and S-based anodes have been widely investigated for LIBs and sodium ion batteries (NIBs) recently due to their high theoretical capacity, fast ion transportation, and decent redox reversibility (Hu et al., 2019; Han et al., 2020). However, there still remains a great challenge owing to its low electronic conductivity and extremely large volume expansion, resulting in poor cyclic stability (Wei et al., 2018).

$SnSe_2$ as a typical two-dimensional (2D) layered material has attracted intensive attention as a promising anode material for LIBs owing to its high theoretical capacity, tunable spacing structures, and non-toxicity (Du et al., 2016; Huang et al., 2018). However, inherently poor conductivity and high-cost synthesis methods of $SnSe_2$ such as complex reaction routes, high temperature, and some toxic reagents limit practical applications (Chen R. et al., 2018; Ren et al., 2018). One of the most popular approaches is to construct $SnSe_2$ nanomaterials with various morphologies and structure, which can effectively improve ion transport kinetics and reduce unavoidable volume expansion. Therefore, it is necessary to search for an effective method to fabricate functional morphology $SnSe_2$ materials with a good electrochemical performance.

Herein, we report a facile colloidal synthetic method to prepare three-dimensional (3D) flowerlike $SnSe_2$ (F-$SnSe_2$). The as-prepared $SnSe_2$ is composed of non-stacking vertical upward hexagonal nanosheets, which can restrain self-agglomeration during a chemical reaction, improve electron and ion transport, and accommodate volume expansion during lithium-ion intercalation/extraction. When employed as LIB anode, the F-$SnSe_2$ exhibits good lithium-ion storage performance with a high reversible capacity of 795 mAh g^{-1} after 100 cycles at 100 mA g^{-1} and superior rate performances, much better than bulk $SnSe_2$ electrode.

EXPERIMENTAL SECTION

Material Synthesis

F-$SnSe_2$ was synthesized by a simple colloid method. First, 0.2 mmol of stannous chloride was put into a 25-ml single-neck flash along with 10-ml oleylamine (OAm). The mixtures were magnetically stirred for 30 min at 90°C to form a milky suspension. After the solution was cooled down to room temperature, 0.4 mmol dibenzyldiselenide was added into the mixture and then heated to 240°C for 2 h with a heating rate of 8°C min^{-1}. Finally, the obtained black solution was washed with ethanol and cyclohexane several times and vacuum dried at 70°C overnight, and the collected sample was marked as F-$SnSe_2$.

Materials Characterization

X-ray diffraction (XRD) was performed on a Smart-lab using Cu Kα radiation from 10 to 90° at a scan rate of 10° min^{-1}. The field-emission scanning electron microscopy (FESEM, Hitachi SU8010) and transmission electron microscopy (TEM, JEOL JEM-2100F) were used to characterize the morphology of the samples. The atomistic structural information and microtopography were characterized using high-resolution (HR) TEM (JEM-2200FS), selected area electron diffraction (SAED), and equipped with an energy-dispersive spectroscopy (EDS) mapping by high-angle annular dark-field scanning transmission electron microscopy (HAADF-STEM). The specific surface area

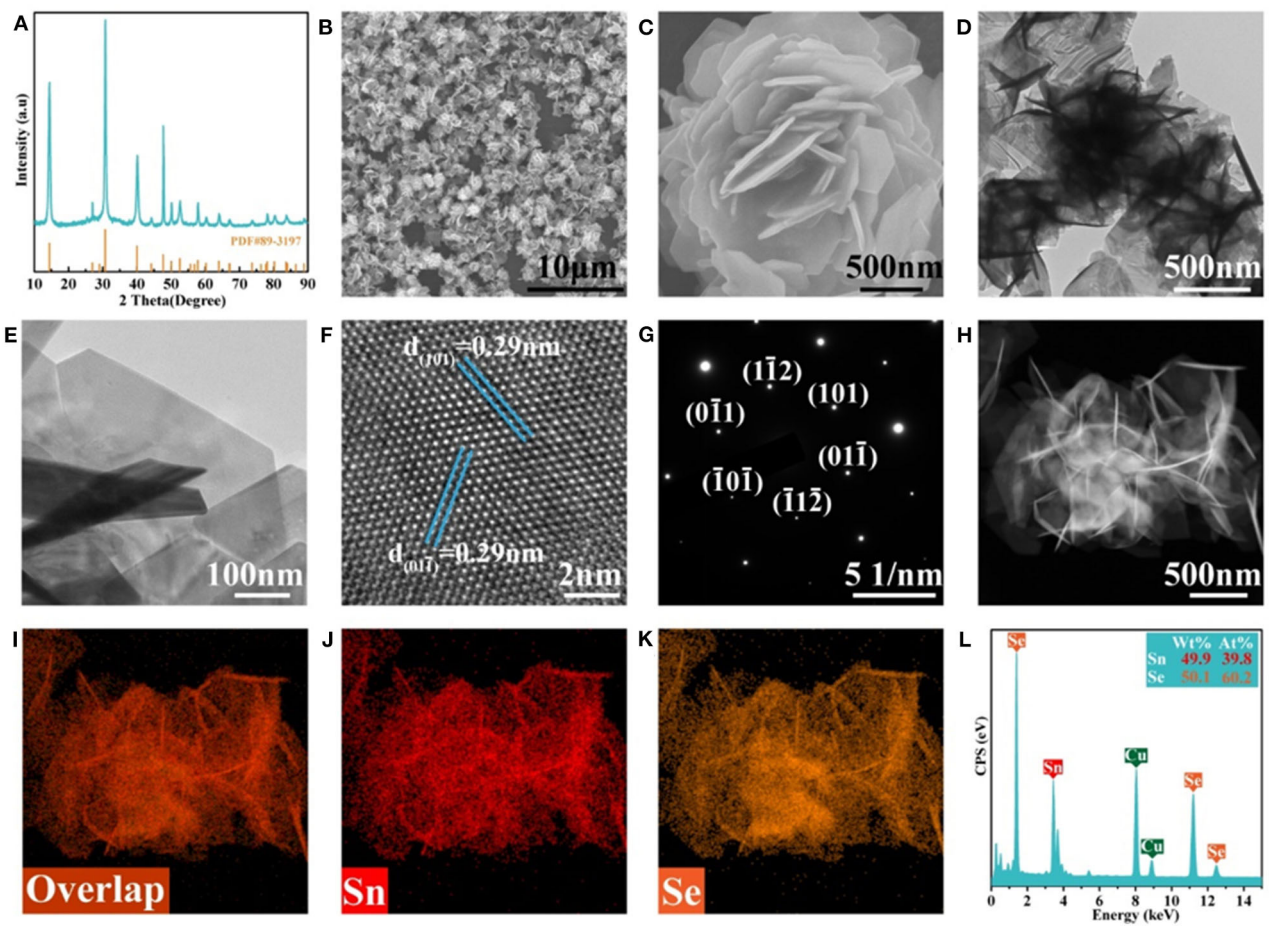

FIGURE 1 | (A) X-ray diffraction (XRD) patterns, **(B,C)** field-emission scanning electron microscopy (FESEM) images, and **(D,E)** transmission electron microscopy (TEM) images of F-$SnSe_2$. **(F)** High-resolution transmission electron microscopy (HRTEM) image of the F-$SnSe_2$ and the corresponding **(G)** selected area electron diffraction (SAED) pattern. **(H)** High-angle annular dark-field scanning transmission electron microscopy (HAADF-STEM) image, **(I–K)** element mapping of Sn and Se and the corresponding **(L)** energy-dispersive spectroscopy (EDS) spectrum.

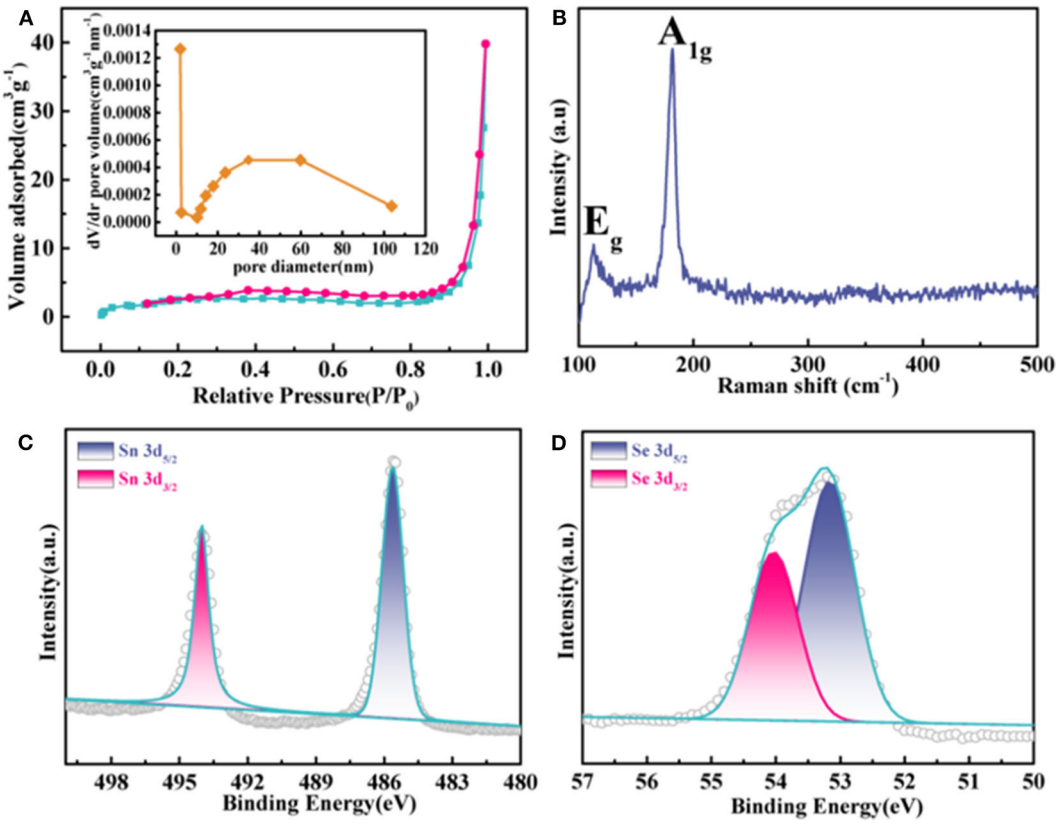

FIGURE 2 | (A) N_2 adsorption–desorption isotherms of F-$SnSe_2$; inset is the corresponding pore size distribution curve. **(B)** Raman spectra and high-resolution X-ray photoelectron spectroscopy (XPS) spectra of **(C)** Sn 3d and **(D)** Se 3d in F-$SnSe_2$.

of samples was degassed for 6 h at 200°C, then nitrogen adsorption was done for 20 h by using the Brunauer–Emmett–Teller (BET) (ASAP 2460) method. Raman spectra (Lab RAM-HR Evolution, 532 nm laser) with a power of 0.2 mW and the exposure time of 1 s and X-ray photoelectron spectroscopy (XPS, AXIS ULTRADLD Scientific) were conducted to reveal the chemical compositions and surface electronic states.

Electrochemical Measurement

The purchased bulk $SnSe_2$ and F-$SnSe_2$ anodes were prepared by pasting a slurry consisting of active material (70 wt%), acetylene black (20 wt%), and polyvinylidene fluoride (PVDF, 10 wt%) in N-methyl-pyrrolidone (NMP) onto a copper foil current collector. After being dried at 80°C in vacuum overnight, they were cut into disks in the diameter of 10 mm with a mass loading of about 1.1 mg cm^{-2}. Then, 2032-type coin cells were assembled in an argon-filled glove box using Whatman GF/D glass fiber filter as a separator, lithium foil as the reference/counter electrode, and electrolyte solution consisted of 1.0 M $LiPF_6$ dissolved in 1:1 volume ratio of ethylene carbonate and diethyl carbonate. A LAND CT2001A multichannel battery tester system was used to measure the Li storage performances within the voltage range of 0.01–2.5 V (vs. Li/Li^+). Cyclic voltammetry (CV, at a scan rate of 0.1 mV s^{-1}) tests and the electrochemical impedance spectroscopy (EIS, frequency range of 0.01–100 kHz) were recorded on a CHI 604E electrochemical workstation (Shanghai Chenhua Corp.).

RESULTS AND DISCUSSION

Figure 1A shows the XRD pattern of the as-prepared F-$SnSe_2$ which possesses a rhombohedral crystal structure (JCPDS No. 89-3197) (Gurung et al., 2016), and the sharp diffraction peaks reveal the high-crystallinity $SnSe_2$ phase. The morphology and nanostructure of F-$SnSe_2$ were investigated *via* the field emission scanning electron microscopy (FESEM) and transmission electron microscopy (TEM). **Figure 1B** shows the SEM image of $SnSe_2$ that presents a uniform nanoflower-like structure, while the purchased bulk $SnSe_2$ shows a multilayer stack structure (**Figure S1**). **Figure 1C** shows that the F-$SnSe_2$ nanoflower shows a self-assembly 3D structure with size in the range of 2–3 μm, which is composed of numerous nanosheets. TEM images (**Figures 1D,E**) illustrate that the size of F-$SnSe_2$ is composed of non-stacking vertical upward hexagonal nanosheets with a size of around 500 nm, which are derived from a preferable growth of $SnSe_2$ along (011) crystal plane (Im et al., 2014). Moreover, the detailed microstructure of F-$SnSe_2$ is further investigated using high-resolution transmission electron microscopy (HRTEM), as shown in **Figure 1F**. The

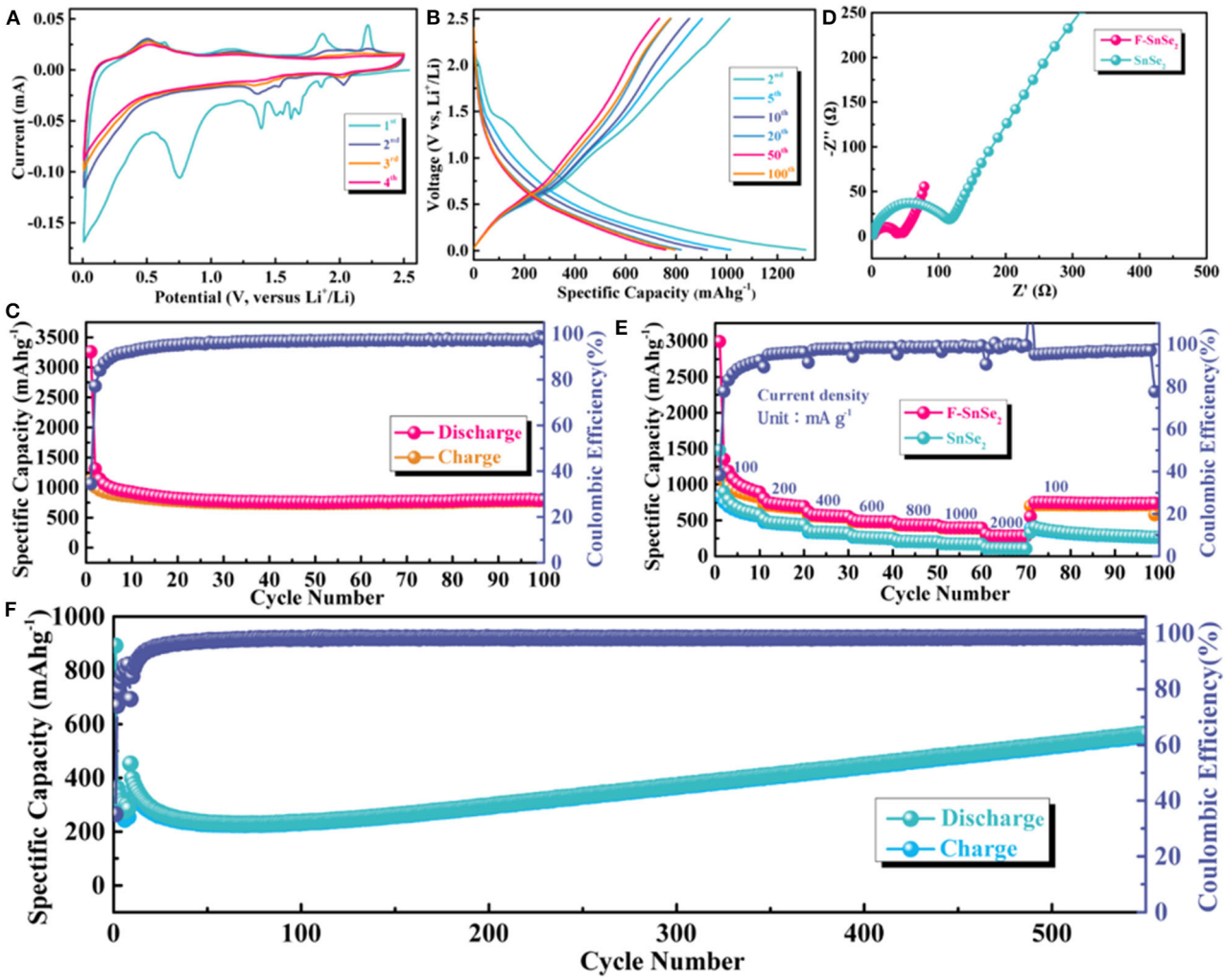

FIGURE 3 | (A) Cyclic voltammogram analysis of F-$SnSe_2$ between 0.01 and 2.5 V at a scan rate of 0.1 mV s^{-1} for lithium-ion batteries (LIBs). **(B)** Charge and discharge curves from 2nd to 100th cycles of F-$SnSe_2$ electrode at a current density of 100 mA g^{-1}. **(C)** Cycling performance of F-$SnSe_2$ electrode at a current density of 100 mA g^{-1}. **(D)** Comparison of electrochemical impedance spectroscopy plots of bulk $SnSe_2$ and F-$SnSe_2$ electrodes. **(E)** Comparison of rate capability of bulk $SnSe_2$ and F-$SnSe_2$ electrodes at various current densities from 100 to 2,000 mA g^{-1}, respectively. **(F)** Long cycling stability of F-$SnSe_2$ electrode at a high current density of 1,000 mA g^{-1}.

(101) and (011) crystal planes with lattice spacing of 0.29 nm (Zhang et al., 2016), which is consistent with the corresponding selected area electron diffraction (SAED) pattern (**Figure 1G**) that shows well-defined spots, suggest a single crystalline nature of the as-grown F-$SnSe_2$. Furthermore, **Figures 1H–K** display the HAADF-STEM and EDS element mapping of F-$SnSe_2$, confirming that Sn and Se elements are distributed uniformly in the whole nanoflower. As expected, EDS analysis (**Figure 1L**) of F-$SnSe_2$ demonstrates that the obtained atomic ratio of Sn to Se approaches 1:2.

Figure 2A exhibits the nitrogen absorption–desorption curve for the F-$SnSe_2$ with type IV isotherms, demonstrating the presence of meso/micropore structures. The corresponding Barrett–Joyner–Halenda (BJH) porosity distribution curve is shown **Figure 2B**, and the calculated specific pore size distribution of F-$SnSe_2$ is estimated to be 1–10 nm. Raman spectra (**Figure 2B**) present two characteristic peaks located at 116 and 185 cm^{-1}, corresponding to the Eg and A1g mode of $SnSe_2$, respectively (Chen M. et al., 2018). The surface chemical states of F-$SnSe_2$ were further studied by XPS as shown in **Figure S2**. Specifically, in the high-resolution XPS spectrum of Sn 3d (**Figure 2C**), two peaks located at 485.9 and 494 eV are assigned to 3d 5/2 and 3d 3/2 of typical values of Sn^{4+} ions, respectively (Saha et al., 2016). Correspondingly, two peaks are observed at 53.2 and 54 eV in the Se 3d 5/2 spectrum (**Figure 2D**), which can be attributed to 3d 5/2 and 3d 3/2 of Se^{2-} in $SnSe_2$ (Zhang et al., 2018).

The lithium storage behaviors of F-$SnSe_2$ were evaluated by CV at a scanning rate of 0.1 mV s^{-1} between 0.01 and

2.5 V (**Figure 3A**). During the first cathodic scan, two large sharp cathodic peaks at around 1.39 and 0.75 V and some small peaks were observed, which disappear in the subsequent cycles, ascribed to lithium intercalation of $SnSe_2$ interlayers without phase transition and the formation of irreversible solid electrolyte interphase (SEI) film (Du et al., 2016). The cathodic peaks that shift to 2.03, 1.52, and 1.35 V in the following scans can be assigned to the conversion and alloying reactions (Yuan et al., 2018). Conversely, two pairs of delithiation peaks at around 0.52 and 1.18 V in all cycles are almost completely overlapped, implying good reversibility of the F-$SnSe_2$ electrode.

Figure S3 and **Figure 3B** show the galvanostatic charge–discharge profiles of the F-$SnSe_2$ electrode at a current density of 100 mA g^{-1} from the first cycle to 100 cycles. The F-$SnSe_2$ electrode delivers an extremely high initial capacity (**Figure S3**), which is attributed to irreversible side reactions with the electrolyte and the formation of the SEI layer on the surface of the F-$SnSe_2$ electrode (Lao et al., 2017). It is worth noting that the initial Coulombic efficiency (CE) should be improved, such as optimizing the electrolyte, pre-lithiation, or compound with carbon matrix to reduce the excess formation of SEI and other irreversible side reactions (Ge et al., 2019; Huang et al., 2020). In addition, the shape of voltage profiles almost overlaps after the initial cycle (**Figure 3B**), which is consistent with the CV results. As shown in **Figure 3C**, the F-$SnSe_2$ anode exhibits excellent cyclic stability, which delivers a high reversible discharge specific capacity of 795 mAh g^{-1} after 100 cycles at 100 mA g^{-1} with a high CE of nearly 100%, while bulk $SnSe_2$ electrode only exhibits a relatively low capacity of 370 mAh g^{-1} after 30 cycles (**Figure S4**).

Furthermore, EIS was performed with F-$SnSe_2$ and bulk $SnSe_2$ anode to investigate the kinetic behavior in LIBs. As indicated in **Figure 3D**, it can be observed that the semicircle of the F-$SnSe_2$ electrode is much smaller than that of the bulk $SnSe_2$ electrode, which suggests lower charge transfer resistance of the F-$SnSe_2$ electrode (Hong et al., 2019). The improved charge transfer is attributed to 3D flower-like nanostructure of F-$SnSe_2$ that enhances fast ion transfer kinetics. As expected, the rate performance of F-$SnSe_2$ was significantly better than that of bulk $SnSe_2$ (**Figure 3E**). For the F-$SnSe_2$ electrode, it could deliver invertible capacity of 892, 694, 554, 483, 430, 393, and 282 mA h g^{-1} at 100, 200, 400, 600, 800, 1,000, and 2,000 mA g^{-1}, respectively. When the current density is switched to 100 mA g^{-1} again, a reversible capacity of 745 mA h g^{-1} is recovered. It is necessary to point out that the partial capacity drop in the first 10 cycles for F-$SnSe_2$ electrode can be ascribed to stabilization of the SEI film and activation process as well as some irreversible side reactions (Li et al., 2018; Chu et al., 2019). In contrast, the capacities at 100, 200, 400, 600, 800, 1,000, and 2,000 mA g^{-1} are 581, 442, 323, 247, 201, 168, and 106 mA h g^{-1} for bulk $SnSe_2$ electrode, respectively. As shown in **Figure 3F**, the F-$SnSe_2$ electrode still delivers a high reversible capacity of 611 mA h g^{-1} after 580 cycles at a high current density of 1,000 mA g^{-1}, demonstrating good long-term cycling stability of F-$SnSe_2$. It is worth mentioning that the capacity fading in the initial 100 cycles can be ascribed to the repetitive volume expansion/contraction that can fracture the SEI layer and expose new active surfaces for SEI growth (Li et al., 2015). Subsequently, high-rate lithiation-induced mechanical degradation can effectively restructure the 3D $SnSe_2$ nanoflower and optimize the SEI, which was defined as reactivation, so the reversible capacity continuously increases during cycling (Qin et al., 2019).

CONCLUSION

In summary, 3D flower-like $SnSe_2$ has been synthesized *via* a colloidal method. This nanoflower is composed of non-stacking vertical upward hexagonal $SnSe_2$ nanosheets, which can improve the ion transfer speed and accommodate the volume expansion during cycling. When evaluated as an anode material for LIBs, the F-$SnSe_2$ electrode delivers significantly enhanced electrochemical performance with high capacity and excellent rate performances. A high capacity of 795 mAh g^{-1} at 100 mA g^{-1} after 100 cycles and a remarkable rate capability of up to 282 mA h g^{-1} at 2 A g^{-1} are obtained. Therefore, this unique structure shows a promising prospect to solve the agglomeration problem.

DATA AVAILABILITY STATEMENT

The raw data supporting the conclusions of this article will be made available by the authors, without undue reservation.

AUTHOR CONTRIBUTIONS

BW and QY designed the experiments and wrote manuscript. JW and SH performed all the experiments. JH and YL helped in chemistry experiments and their design, and the chemical analysis. BW, QY, and JW helped in discussion, evaluation, and restructuring of the findings. All authors contributed in manuscript editing.

FUNDING

This work was supported by the National Natural Science Foundation of China (Grant Nos. 11574060, 51974103), the Natural Science Foundation of Hebei Province (E2019208308, E2019208179), the Science Foundation of University of Hebei Province (BJ2019036, ZD2019062), and the Science Research and Development Program of Shijiazhuang (181790411A).

SUPPLEMENTARY MATERIAL

The Supplementary Material for this article can be found online at: https://www.frontiersin.org/articles/10.3389/fchem.2020.00590/full#supplementary-material

REFERENCES

Chen, K., Wang, X., Wang, G., Wang, B., Liu, X., Bai, J., et al. (2018). A new generation of high performance anode materials with semiconductor heterojunction structure of SnSe/SnO_2@Gr in lithium-ion batteries. *Chem. Eng. J.* 347, 552–562. doi: 10.1016/j.cej.2018.04.125

Chen, M., Li, Z., Li, W., Shan, C., Li, W., Li, K., et al. (2018). Large-scale synthesis of single-crystalline self-standing $SnSe_2$ nanoplate arrays for wearable gas sensors. *Nanotechnology* 29:455507. doi: 10.1088/1361-6528/aade32

Chen, R., Li, S., Liu, J., Li, Y., Ma, F., Liang, J., et al. (2018). Hierarchical Cu doped SnSe nanoclusters as high-performance anode for sodium-ion batteries. *Electrochim. Acta* 282, 973–980. doi: 10.1016/j.electacta.2018.07.035

Chu, J., Wang, W. A., Feng, J., Lao, C. Y., Xi, K., Xing, L., et al. (2019). Deeply nesting zinc sulfide dendrites in tertiary hierarchical structure for potassium ion batteries: enhanced conductivity from interior to exterior. *ACS Nano* 13, 6906–6916. doi: 10.1021/acsnano.9b01773

Du, C. F., Li, J. R., and Huang, X. Y. (2016). Microwave-assisted ionothermal synthesis of $SnSe_x$ nanodots: a facile precursor approach towards $SnSe_2$ nanodots/graphene nanocomposites. *RSC Adv.* 6, 9835–9842. doi: 10.1039/C5RA24500A

Ge, P., Li, S., Xu, L., Zou, K., Gao, X., Cao, X., et al. (2019). Hierarchical hollow-microsphere metal-selenide@carbon composites with rational surface engineering for advanced sodium storage. *Adv. Energy Mater.* 9:1803035. doi: 10.1002/aenm.201803035

Gurung, A., Naderi, R., Vaagensmith, B., Varnekar, G., Zhou, Z., Elbohy, H., et al. (2016). Tin selenide—multi-walled carbon nanotubes hybrid anodes for high performance lithium-ion batteries. *Electrochim. Acta* 211, 720–725. doi: 10.1016/j.electacta.2016.06.065

Han, L., Wu, S., Hu, Z., Chen, M., Ding, J., Wang, S., et al. (2020). Hierarchically porous MoS_2-carbon hollow rhomboids for superior performance of the anode of sodium-ion batteries. *ACS Appl. Mater. Interfaces* 12, 10402–10409. doi: 10.1021/acsami.9b21365

He, D., Li, P., Wang, W., Wan, Q., Zhang, J., Xi, K., et al. (2020). Collaborative design of hollow nanocubes, *in situ* cross-linked binder, and amorphous void@SiO_x@C as a three-pronged strategy for ultrastable lithium storage. *Small* 16, 1–12. doi: 10.1002/smll.201905736

Hong, Y., Mao, W., Hu, Q., Chang, S., Li, D., Zhang, J., et al. (2019). Nitrogen-doped carbon coated SnO_2 nanoparticles embedded in a hierarchical porous carbon framework for high-performance lithium-ion battery anodes. *J. Power Sources* 428, 44–52. doi: 10.1016/j.jpowsour.2019.04.093

Hu, Z., Tai, Z., Liu, Q., Wang, S.-W., Jin, H., Wang, S., et al. (2019). Ultrathin 2D TiS_2 nanosheets for high capacity and long-life sodium ion batteries. *Adv. Energy Mater.* 9:1803210. doi: 10.1002/aenm.201803210

Huang, H., Xu, R., Feng, Y., Zeng, S., Jiang, Y., Wang, H., et al. (2020). Sodium/potassium-ion batteries: boosting the rate capability and cycle life by combining morphology, defect and structure engineering. *Adv. Mater.* 32:e1904320. doi: 10.1002/adma.201904320

Huang, Z., Liu, B., Kong, D., Wang, Y., and Yang, H. (2018). $SnSe_2$ quantum dot/rGO composite as high performing lithium anode. *Energy Storage Mater.* 10, 92–101. doi: 10.1016/j.ensm.2017.08.008

Im, H. S., Lim, Y. R., Cho, Y. J., Park, J., Cha, E. H., and Kang, H. S. (2014). Germanium and tin selenide nanocrystals for high-capacity lithium ion batteries: comparative phase conversion of germanium and tin. *J. Phys. Chem. C* 118, 21884–21888. doi: 10.1021/jp507337c

Jiang, Y., Song, D., Wu, J., Wang, Z., Huang, S., Xu, Y., et al. (2019). Sandwich-like SnS_2/graphene/SnS_2 with expanded interlayer distance as high-rate lithium/sodium-ion battery anode materials. *ACS Nano* 13, 9100–9111. doi: 10.1021/acsnano.9b03330

Lao, M., Zhang, Y., Luo, W., Yan, Q., Sun, W., and Dou, S. X. (2017). Alloy-based anode materials toward advanced sodium-ion batteries. *Adv. Mater.* 29, 1–23. doi: 10.1002/adma.201700622

Lee, D. H., and Park, C. M. (2017). Tin selenides with layered crystal structures for li-ion batteries: interesting phase change mechanisms and outstanding electrochemical behaviors. *ACS Appl. Mater. Interfaces* 9, 15439–15448. doi: 10.1021/acsami.7b01829

Li, G., Xu, L., Zhai, Y., and Hou, Y. (2015). Fabrication of hierarchical porous $MnCo_2O_4$ and $CoMn_2O_4$ microspheres composed of polyhedral nanoparticles as promising anodes for long-life LIBs. *J. Mater. Chem. A* 3, 14298–14306. doi: 10.1039/C5TA03145A

Li, L., Wang, H., Xie, Z., An, C., Jiang, G., and Wang, Y. (2020). 3D graphene-encapsulated nearly monodisperse Fe_3O_4 nanoparticles as high-performance lithium-ion battery anodes. *J. Alloys Compd.* 815:152337. doi: 10.1016/j.jallcom.2019.152337

Li, Z., Zhao, H., Lv, P., Zhang, Z., Zhang, Y., Du, Z., et al. (2018). Watermelon-like structured SiO_x-TiO_2@C nanocomposite as a high-performance lithium-ion battery anode. *Adv. Funct. Mater.* 28:1605711. doi: 10.1002/adfm.201605711

Qin, M., Zhang, Z., Zhao, Y., Liu, L., Jia, B., Han, K., et al. (2019). Optimization of von mises stress distribution in mesoporous α-Fe_2O_3/C hollow bowls synergistically boosts gravimetric/volumetric capacity and high-rate stability in alkali-ion batteries. *Adv. Funct. Mater.* 29:1902822. doi: 10.1002/adfm.201902822

Ren, X., Wang, J., Zhu, D., Li, Q., Tian, W., Wang, L., et al. (2018). Sn-C bonding riveted SnSe nanoplates vertically grown on nitrogen-doped carbon nanobelts for high-performance sodium-ion battery anodes. *Nano Energy* 54, 322–330. doi: 10.1016/j.nanoen.2018.10.019

Saha, S., Banik, A., and Biswas, K. (2016). Few layer nanosheets of n-type $SnSe_2$. *Chem. A Eur. J.* 22, 15634–15638. doi: 10.1002/chem.201604161

Wang, W., Huang, H., Wang, B., Qian, C., Li, P., Zhou, J., et al. (2019). A new dual-ion battery based on amorphous carbon. *Sci. Bull.* 64, 1634–1642. doi: 10.1016/j.scib.2019.08.021

Wei, Z., Wang, L., Zhuo, M., Ni, W., Wang, H., and Ma, J. (2018). Layered tin sulfide and selenide anode materials for Li- and Na-ion batteries. *J. Mater. Chem. A* 6, 12185–12214. doi: 10.1039/C8TA02695E

Yuan, H., Jin, Y., Lan, J., Liu, Y., Yu, Y., and Yang, X. (2018). *In situ* synthesized SnSe nanorods in a SnO_x@CNF membrane toward high-performance freestanding and binder-free lithium-ion batteries. *Inorg. Chem. Front.* 5, 932–938. doi: 10.1039/C7QI00762K

Zhang, F., Xia, C., Zhu, J., Ahmed, B., Liang, H., Velusamy, D. B., et al. (2016). $SnSe_2$ 2D anodes for advanced sodium ion batteries. *Adv. Energy Mater.* 6, 1–10. doi: 10.1002/aenm.201601188

Zhang, Y., Xu, Y., Ji, Y., Wang, X., Li, J., Liu, H., et al. (2019). Constructing radially oriented macroporous spheres with central cavities as ultrastable lithium-ion battery anodes. *Energy Storage Mater.* 17, 242–252. doi: 10.1016/j.ensm.2018.07.011

Zhang, Y., Yang, J., Zhang, Y., Li, C., Huang, W., Yan, Q., et al. (2018). Fe_2O_3/SnSSe hexagonal nanoplates as lithium-ion batteries anode. *ACS Appl. Mater. Interfaces* 10, 12722–12730. doi: 10.1021/acsami.8b01537

Conflict of Interest: The authors declare that the research was conducted in the absence of any commercial or financial relationships that could be construed as a potential conflict of interest.